Geophysical Journal International

Geophys. J. Int. (2021) **0,** 1–0
Advance Access publication 2021 April 12
GJI Geomagnetism, Rock Magnetism and Palaeomagnetism

doi: 10.1093/gji/ggab138

Magnetic hysteresis of magnetite at high temperature: grain size variation

David J. Dunlop

Department of Physics, University of Toronto, Toronto, ON M5S1A7, Canada. E-mail: dunlop@physics.utoronto.ca

Accepted 2021 April 8. Received 2021 March 29; in original form 2021 January 22

SUMMARY

Thermoremanent magnetization (TRM), the primary magnetic memory of igneous rocks, depends for its stability through geologic time on mineral carriers with high coercivities and high unblocking temperatures. The palaeomagnetic record of past magnetic field directions and intensities is the key to unraveling Earth's tectonic history. Yet we still do not fully understand how the familiar mineral magnetite, in the micrometer grain size range typically responsible for stable TRM, acquires and holds its signal. Direct indicators of magnetite remanence-carrying capacity and coercivity at high temperature T are saturation remanence relative to saturation magnetization M_{rs}/M_s and coercive force H_c. This study is the first to measure the variation of these hysteresis properties for magnetite, from room temperature to the Curie point, across the entire size range from 25 nm to 135 μm, covering superparamagnetic, single-domain, vortex, pseudo-single-domain and multidomain magnetic behaviour. The paper focuses on: (1) $H_c(T)$ and $M_{rs}(T)$ observations and their reproducibility; (2) mathematical relationships of $H_c(T)$ and $M_{rs}(T)$ to $M_s(T)$, used in modelling TRM and for unbiased comparisons of thermal variations; (3) the shapes of magnetite grains and the number of domains they contain, revealed by demagnetizing factors $N = H_c/M_{rs}$ and (4) the grain size dependences of H_c and M_{rs} at ordinary and elevated T, delineating domain structure changes and mechanisms of coercivity.

Key words: Magnetic mineralogy and petrology; Rock and mineral magnetism.

1 INTRODUCTION

An earlier paper (Dunlop 2021: paper 1) reported hysteresis properties of magnetites with sizes d from 0.025–0.065 to 135 μm at temperatures T from 25 to 585 °C. Corresponding domain structures ranged from superparamagnetic (SP), single-domain (SD) and vortex states with permanent magnetic moments through few-domain pseudo-single-domain (PSD) structures to multidomain (MD) grains with variable moments due to displaced domain walls (DWs).

PSD is here taken to be distinct from vortex [see Roberts *et al.* (2017) for a contrary view]. Experimentally, magnetite grains between 1 and 15 μm in size are observed to contain domains and DWs. For example, three to five body domains were observed by magnetic force microscopy in 5, 8, 12 and 13 μm magnetite crystals (Pan *et al.* 2002). Geiss *et al.* (1996), using the Bitter powder method, detected DWs in magnetite throughout the 0.5–10 μm range. The experimental evidence is summarized in Özdemir & Dunlop (2006, their figs 13, 14) and Dunlop & Özdemir (2015, their fig. 7).

Vortices undoubtedly exist in >1 μm magnetite, but in some of these grains DWs have found enough 'elbow room' to develop, using vortices as nuclei (Nagy *et al.* 2019). A grain in a vortex state has a small moment compared to an SD grain. The core vortex line carries the moment while the bulk of the vortex has a null net moment. Vortices are thus unlikely to bridge the gap in explaining the gradual rather than abrupt change in remanence (and coercivity) magnitudes between SD and MD states. Few-domain grains are a more likely bridge. In addition to the domains themselves, the individual DWs have moments approaching SD magnitudes (Dunlop 1977). The cramped space in which the DWs find themselves inhibits wall motion, explaining enhanced coercivities. Whether or not this scenario is correct in detail, domains and DWs are experimentally the norm in the classic 1–15 μm PSD range (Stacey 1962; Parry 1965).

Nagy *et al.*'s (2019) modelling of domain structures in cuboctahedral magnetites of increasing size shows that proto-domains begin to develop below 1 μm. Recognizable domains separated by 70.5° DWs (usually associated with closure domains) are well established in 1.5 and 2.7 μm grains. When model grain sizes are reduced, these structures persist until 0.7 μm. Thus the vortex → PSD (broad-walled MD) transition is ≈0.7–1 μm, as the experimental evidence in the present paper will confirm. Nagy *et al.*'s measured DW widths of 0.12–0.15 μm would be narrow in large MD grains but in 1–2.7 μm grains are broad, comparable to the domain widths.

Despite widely contrasting domain states, paper 1 found similar temperature variations of key hysteresis parameters like saturation remanence M_{rs} and coercive force H_c over the sample set. The

© The Author(s) 2021. Published by Oxford University Press on behalf of The Royal Astronomical Society.

Table 1. Size and shape determinations for the sieved and centrifugally separated fractions of PQ magnetite.

Nominal grain size (μm)	Mean grain width (μm)	Dispersion (μm)	Axial ratio
135	125–150*	—	—
110	100–125*	—	—
20	19.95	±4.60	1.52
14	14.05	±3.69	1.39
9	8.93	±2.69	1.45
6	5.84	±2.23	1.46
3	2.97	±1.17	1.49
1	0.956	±0.502	1.43
0.6	0.615	±0.304	1.49

*Range of mesh sizes.

universal decrease in the squareness ratio M_{rs}/M_s (M_s being saturation magnetization) at high T suggests that grains cooling from the Curie point might denucleate domains and/or vortices, becoming more SD-like in the process. However, the decrease of M_{rs}/M_s at high T could also be due to thermal activation (SD or vortex → SP) and/or increased mobility of walls at high T.

The purpose of this paper is to make a quantitative analysis of the results of paper 1. Topics include: (1) microstructural changes in the magnetites indicated by irreversibility between initial and repeat temperature runs; (2) the description of $M_{rs}(T)$ and $H_c(T)$ in terms of $M_s(T)$, a material property independent of domain structure; (3) grain demagnetizing factors $N = H_c/M_{rs}$, which shed light on grain shape and the number of domains and (4) the grain size dependences of M_{rs} and H_c at fixed T, from which one can infer domain structure ranges at ordinary and elevated temperatures as well as mechanisms of domain-wall pinning.

2 PROCEDURES AND SAMPLES

Experimental methods and samples were described in detail in paper 1. In brief, hysteresis loops of magnetization M versus magnetic field H were measured with a Princeton Measurements Corporation vibrating-sample magnetometer (VSM) every 20 °C from 25 to 585 °C (0.5 T maximum field). Flowing He gas was used to inhibit oxidation at high T. Initial susceptibility k_0 was recorded using a Geofyzika KLY-2 Kappabridge every ≈3 °C in heating from 20 to 600 °C and cooling to 50 °C. k_0 decreased rapidly to zero just below the magnetite Curie point, $T_C = 580$ °C, except for sample TK49, described next, which had $T_C \approx 550$ °C (Dunlop 2014).

Natural magnetites included plagioclase separate TK49 (Dunlop *et al.* 2005) containing fine magnetite inclusions with SD hysteresis properties at 20 °C ($M_{rs}/M_s = 0.455$, $\mu_0 H_c = 53.6$ mT) and dark minerals separate TK128 containing magnetite with large PSD to small MD hysteresis at 20 °C ($M_{rs}/M_s = 0.029$, $\mu_0 H_c = 3.1$ mT). Hydrothermal magnetite FH3A (Heider *et al.* 1987) was included as a representative of magnetites with low levels of internal stress; the grain size spectrum peaks near 3 μm with a tail to smaller sizes.

Massive magnetite ore from Ishpeming, MI and single crystals from Bancroft, ON (Princess Quarry, PQ) provided MD magnetite. Some PQ crystals were crushed and sieved into coarse-grained fractions (mean sizes 110 and 135 μm). The residue was centrifugally separated into seven finer-grained fractions (mean sizes from 0.6 to 20 μm, Table 1; see Dunlop *et al.* 2019 for details). All PQ samples had $T_C = 580$ °C.

Commercial magnetites from the Wright Company (Jackson *et al.* 1990; Yu *et al.* 2002, 2004; Carter-Stiglitz *et al.* 2006) were included to fill gaps in grain size coverage. The submicron Wright magnetites had Curie points of 590–600 °C, evidence of surface oxidation of the grains to maghemite.

3 M_{rs} AND H_c DATA

Fig. 1 presents examples of M_{rs}, H_c and M_s data measured at 20 °C intervals of temperature T from 25 to 585 °C. In general, M_{rs} and H_c values drop more rapidly with increasing T than does M_s M_s values are reproducible between the first and subsequent heatings but M_{rs} and H_c values frequently are not. Analyses in Sections 4–6 use stabilized values measured in the second heating. Most often M_{rs} and H_c values decrease with T at similar rates, as expected if $\boldsymbol{M}$ is controlled by the internal demagnetizing field $\boldsymbol{H_d} =—N\boldsymbol{M}$, where N is grain demagnetizing factor. For the finest grains, $H_c(T)$ decreases more rapidly than $M_{rs}(T)$, as expected for thermally activated remanence unblocking. These observations guide quantitative analyses of $H_c(T)$ and $M_{rs}(T)$ in terms of $M_s(T)$ in Section 4 and computation of demagnetizing factors in Section 5. Section 6 presents explicit grain size dependences of stabilized H_c and M_{rs} data at elevated T.

How reproducible are the hysteresis data? FH3A (Fig. 1a) was produced hydrothermally. Despite its low levels of internal strain (Heider *et al.* 1987), M_{rs} and H_c measurements below the $T =$ 205 °C step are very different between runs 1 and 2. Only above $T = 305$ °C do the data from the two runs converge. M_s data from the two runs are similar at all steps and match the standard $M_s(T)$ curve of magnetite (Dunlop & Özdemir 1997, figs 2.4 and 3.5), reaching zero around 580 °C. Thus chemical alteration is not the cause of the non-reproducible M_{rs} and H_c data from run 1. A third set of measurements gave M_{rs} and H_c results very similar to those of run 2. Apparently any microstructural changes were complete in the first heating, likely below 300 °C.

The Ishpeming magnetite ore has the coarsest grain sizes of all the samples (paper 1, Table 1) and formed in a low-stress environment. It nevertheless displays the same patterns as FH3A in its M_{rs}, H_c and M_s data (Fig. 1b). Where M_{rs} and H_c increased by 20 per cent between the 65 and 105 °C steps for FH3A, the ≈ 15 per cent increase for the Ishpeming ore occurs between 105 and 145 °C, with the run 1 and 2 data merging above the 245 °C step. M_s changes reversibly and matches the magnetite $M_s(T)$ curve. A curious feature of the data is that M_{rs} and M_s both reach zero by 580 °C but H_c does not. It retains around 40 per cent of its room-temperature value, although this is very small in absolute terms: 0.35 mT. Similar H_c residuals appear in the data for FH3A (∼10 per cent or 0.9 mT) and for TK128, magnetite inclusions of presumed 20–40 μm size (∼20 per cent or 0.6 mT: paper 1, Fig. 2d). They could indicate traces of a mineral with small M_s but large H_c (hematite?). It is not likely that the H_c residuals are an artefact introduced by the VSM software because they are not seen in the data for synthetic and crushed natural magnetites.

Examples of data for magnetites crushed from large natural crystals and centrifugally sorted into size fractions appear in Figs 1(c) and (d). Other examples, for mean grain sizes of 0.6, 1 and 14 μm, appear in Dunlop (2014, Fig. 4). Results follow the same pattern for all five grain sizes. M_s data are identical or nearly so for the two heating runs and are a close match for $M_s(T)$ of magnetite (Curie temperatures T_C between 575 and 580 °C). M_{rs} and H_c data differ substantially between the two runs, however. In run 1, both parameters change in similar ways, dropping by ∼20 per cent between the 125 and 265 °C steps, then briefly leveling out before an inflection point near 305 °C, past which the data again descend steeply. In run 2, the starting values of M_{rs} and H_c are much lower: 50–55 per

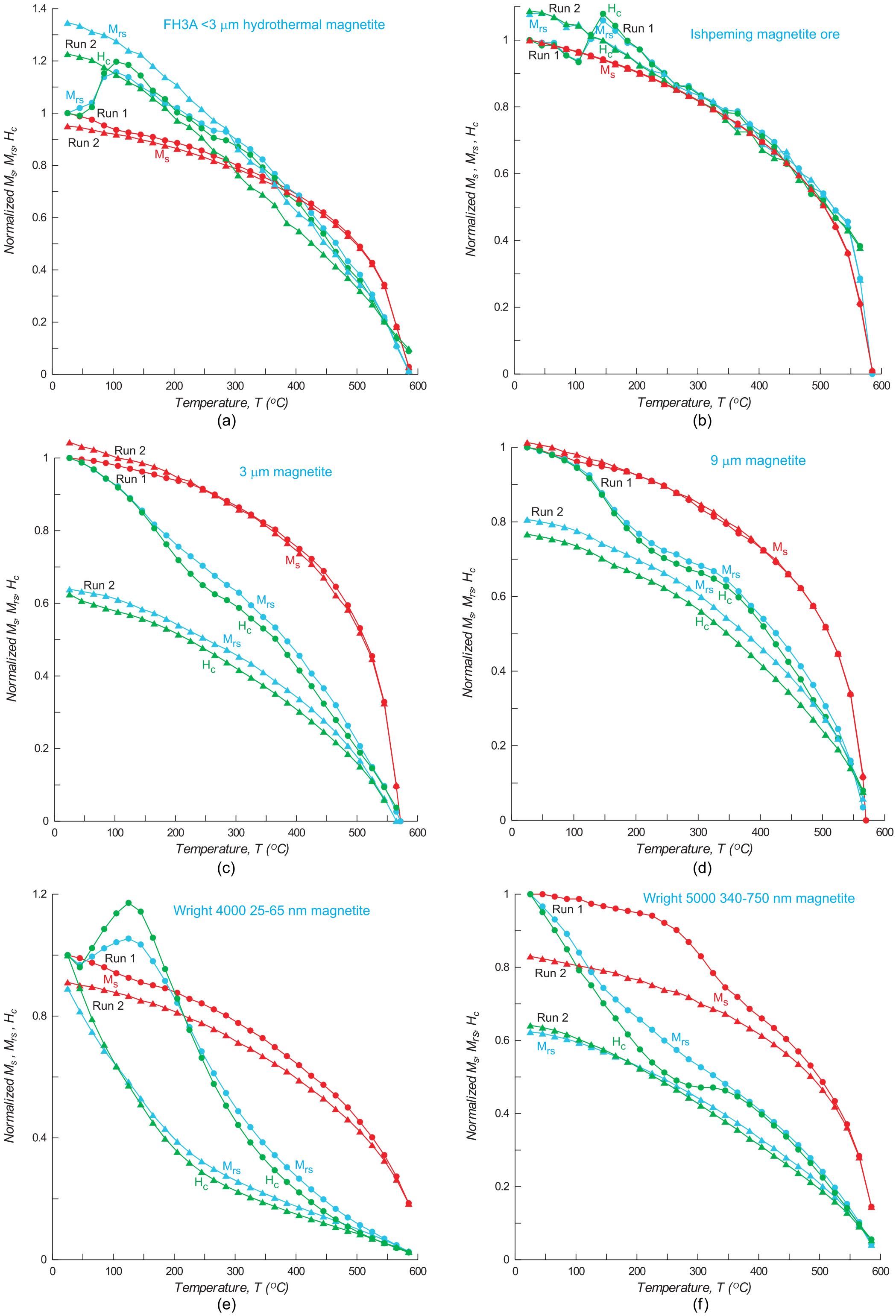

Figure 1. Changes in the parameters M_s, M_{rs} and H_c, measured in hysteresis loops at successively higher temperatures, between heating run 1 (circles; previously unheated samples) and a subsequent heating (run 2; triangles). Measurements are normalized to initial values in run 1. (a) $M_s(T)$ changes slightly after a first heating to 585 °C for hydrothermal magnetite FH3A, probably as a result of minor oxidation, while $M_{rs}(T)$ and $H_c(T)$ change significantly. The increases in both parameters between the 45 and 105 °C heating steps in run 1 are replaced by a regular decrease with increasing T in later runs. (b) Coarse-grained Ishpeming magnetite behaves similarly to FH3A, with sharp increases in M_{rs} and H_c values between the 105 and 145 °C steps in run 1. The data from both runs merge in the 245 °C and higher steps. H_c retains an anomalous non-zero value at the magnetite Curie point where M_s and $M_{rs} \rightarrow 0$. (c), (d) Samples 3 U and 9 U display irreversible behaviour common to all the crushed magnetites: a plunge in M_{rs} and H_c values between the 125 and 185 °C steps followed by an inflection around 305 °C in run 1; and a regular decrease of $M_{rs}(T)$ and $H_c(T)$ from much lower initial values in run 2. The drop in initial values increases with decreasing grain size. (e), (f) Examples of more exotic behaviour in Wright 4000 and 5000 synthetic submicron magnetites (see discussion in text).

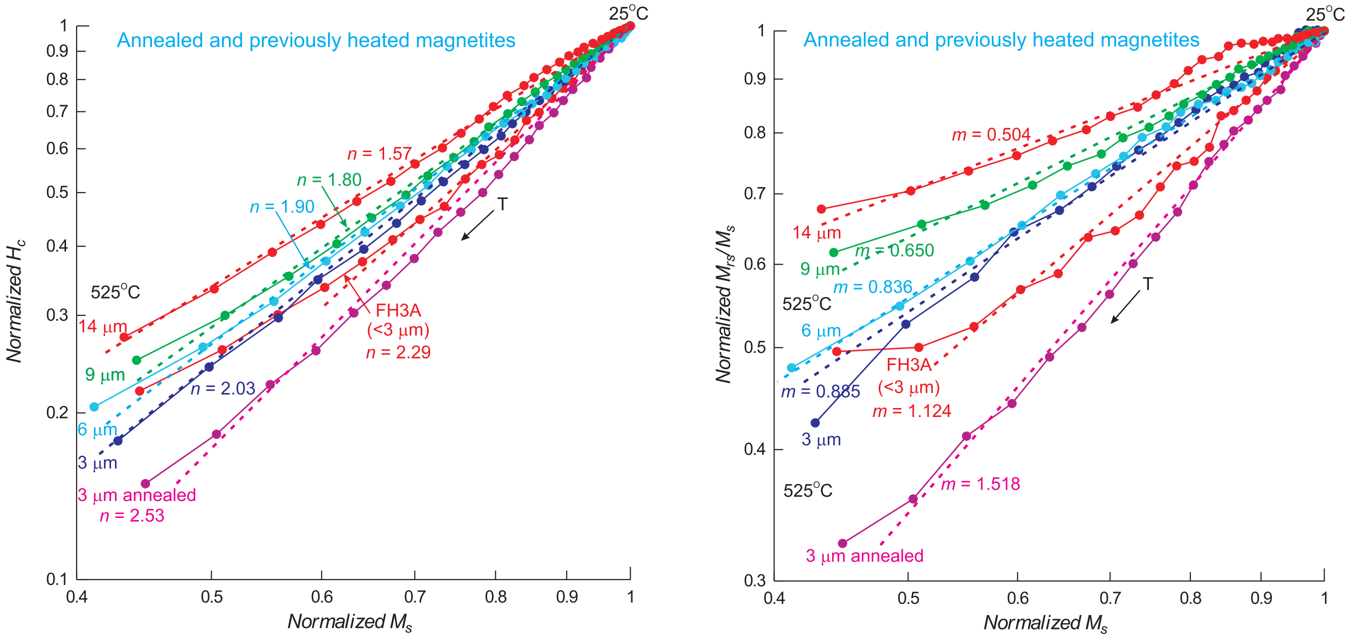

(a) (b)

Figure 2. Bilogarithmic plots of (a) H_c versus M_s data and (b) M_{rs}/M_s versus M_s data, measured at temperatures from 25 to 525 °C and normalized to 25 °C values, for magnetites with mean sizes between 3 and 14 µm. The plots are intended to test the mathematical representations $H_c(T) \sim [M_s(T)]^n$ and $M_{rs}(T)/M_s(T) \sim [M_s(T)]^m$ (eqs 1 and 2). If these power laws are valid, the plots should be linear, with slopes n and m, respectively. Most samples in this size interval do have linear behaviour; deviations from linearity occur mainly above 500 °C.

cent (0.6 µm), 60 per cent (1 µm), 65 per cent (3 µm), 80 per cent (9 µm) and 85 per cent (14 µm). The data descend smoothly and monotonically, but only begin to merge with the run 1 values at the highest T steps, generally well above 500 °C. In other words, M_{rs} and H_c are substantially reduced as a result of the first heating at all measurement temperatures, not just below 300 °C as was the case for FH3A and the Ishpeming ore.

The final two examples (Figs 1e and f), for submicron synthetic magnetites from the Wright Company, have more exotic temperature variations. Wright 4000 contains a large fraction of ultrafine magnetite of SP and small SD size. The finest grains are initially somewhat oxidized, as evidenced by a Curie point $T_C > 580$ °C. Inversion of near-maghemite surface layers of grains or direct oxidation of magnetite to hematite at or near T_C would account for the irreversible drop in M_s values between runs 1 and 2, by ~10 per cent at each T step. The magnetite-like shape of the $M_s(T)$ curve is unchanged. In run 1 M_{rs} and H_c at first increase in successive heating steps, reaching a peak at 125 °C reminiscent of the FH3A and Ishpeming data (Figs 1a and b). However, the measurements then plunge and only begin to level out as T_C approaches, unlike all other samples where the M_{rs} and H_c data trace out convex-up curves and drop most rapidly near T_C.

In run 2, the Wright 4000 M_{rs} and H_c data trace out convex-down curves over the entire T range from 25 to 585 °C. These are similar in shape to the run-1 data plots above the 205 °C step but individual M_{rs} and H_c values are much lower. The unusual shape suggests thermal unblocking of fine SD grains, only slightly larger than SP size at 25 °C, over the entire T range to the Curie point but particularly below 250 °C. The very substantial decrease in M_{rs} and H_c values at each T step is unlikely to be due to annealing out of microstress, as in the case of the crushed magnetites of Figs 1(c) and (d). Possibly inversion of grain surface layers promotes cracking of the grain interiors. The reduction in effective particle size would reduce both M_{rs} and H_c.

Most Wright 5000 magnetite grains are well above SD size and probably contain vortices and/or incipient domain walls. Run-1 M_s values (Fig. 1f) are almost 20 per cent higher than run-2 values up to 245 °C but most of the difference between the two runs disappears by 345 °C. Why grains averaging ~0.5 µm in size should suffer major oxidation at such low temperatures is unclear. M_{rs} and H_c data from run 1 are non-reproducible and trace out curves reminiscent of those of the 3 and 9 µm crushed magnetites (Figs 1c and d). The H_c curve in particular is strongly inflected and levels out entirely between the 285 and 345 °C steps. In run 2, M_{rs} and H_c values begin from 60 to 65 per cent of the initial run-1 values and decrease in a smooth regular fashion at all steps up to 585 °C. Both the initial values and the normalized data plots closely resemble those of the 1 and 3 µm crushed magnetites. The only notable difference is that the Wright 5000 magnetites are maghemitized, with Curie points close to 600 °C.

4 NUMERICAL RELATIONS AMONG $M_{rs}(T)$, $H_c(T)$ AND $M_s(T)$

In theoretical applications, for example theories of the acquisition of thermoremanent magnetization (TRM, Néel 1955; Everitt 1962; Schmidt 1973; Berndt & Chang 2018), the temperature variations $H_c(T)$ and $M_{rs}(T)$ are described in terms of a power-law dependence on $M_s(T)$:

$$H_c(T), M_{rs}(T) \sim [M_s(T)]^n. \tag{1}$$

Experimentally (Figs 1a–f, stabilized run 2 data) normalized $H_c(T)$ and $M_{rs}(T)$ data are very similar. The same index n gives a good description of either temperature variation. (For a theoretical explanation of this observation see Section 5).

Table 2. Indices n and m from the power laws $H_c(T) \sim [M_s(T)]^n$ and $M_{rs}(T)/M_s(T) \sim [M_s(T)]^m$ and demagnetizing factors N (in cgs emu) inferred from experimental values of $H_c(T)/M_{rs}(T)$.

Sample	Grain size (μm)	n	m	n—m	N
TK49 plagioclase	2.83	1.02	1.81		
Wright 112 978	0.19–0.44	3.12	1.43	1.69	
Wright 5000	0.34–0.75	2.40	1.03	1.37	
0.6 U*	av. 0.62	2.54	1.14	1.40	
Wright 3006	1.0–1.1	2.11	1.00	1.11	2.0
1 U*	av. 0.96	2.22	1.06	1.16	1.85
3 U*	av. 3.0	2.03	0.885	1.145	2.0
3 A*	av. 3.0	2.53	1.52	1.01	1.8
FH3A hydrothermal	≤ 3	2.29	1.125	1.165	2.1
6 U*	av. 5.8	1.90	0.836	1.064	1.9
9 U*	av. 8.9	1.80	0.650	1.15	2.0
14 U*	av. 14.1	1.57	0.504	1.066	1.95
20 U*	av. 20.0	2.8			
Wright 04 1183	18.3–40	1.78	0.680	1.10	2.1
TK128 dark minerals	1.81	0.722	1.088	2.2	
Wright 112 982	16.9–37.5	1.74	0.508	1.232	2.2
110 U*	100–125	1.50	0.464	1.036	4.0
135 U*	125–150	1.14	0.24	0.90	3.2
Ishpeming ore	2.85				

*U, A denote samples that were unannealed or annealed at 700 °C, respectively, before the first heating.

The derived parameter M_{rs}/M_s (the squareness ratio) is of special interest as a domain-state indicator. In view of (1), we can expect a power-law relationship

$$M_{rs}(T)/M_s(T) \sim [M_s(T)]^m. \tag{2}$$

We anticipate that $m = n–1$, n and $–1$ being the respective indices for $M_{rs}(T)$ and $1/M_s(T)$.

Relations (1) and (2) are put to the test in Figs 2(a) and (b) for samples with mean grain sizes from 3 to 14 μm (PSD range). Other sizes were tested as well but the most linear behaviour of both $H_c(T)$ vs $M_s(T)$ and $M_{rs}(T)/M_s(T)$ vs $M_s(T)$ on bilogarithmic plots was for these samples. Best-fitting values of n and m are given in Table 2. MD magnetites 30–135 μm in size had linear $H_c(T)$ versus $M_s(T)$ plots but sometimes noisy $M_{rs}(T)/M_s(T)$ versus $M_s(T)$ plots. Samples with grain sizes $\leq$1 μm had systematically curved log–log plots attributable to the effects of thermal unblocking (SD→SP) on $H_c(T)$ and $M_{rs}(T)$; values of n and m from these samples are approximate.

The data plotted in Figs 2(a) and (b) are for run 2 (‘previously heated’) except for sample 3 A (‘3 μm annealed’) which was heated for several hours at 700 °C and cooled to 20 °C over a period of ≈2 hr before measurements began. All samples except FH3A have logarithmic $H_c(T)$ versus $M_s(T)$ plots that are linear up to the penultimate temperature step (Fig. 2a). The logarithmic $M_{rs}(T)/M_s(T)$ versus $M_s(T)$ plots (Fig. 2b) are more scattered, the ordinate being a ratio of two measured quantities with associated noise, plotted on a scale magnified almost two-fold compared to Fig. 2(a). They are nevertheless essentially linear.

Table 2 summarizes the power-law indices n and m for the PSD samples of Fig. 2 and for SP/SD/vortex and MD size magnetites whose data are not shown. A first observation is that except for 135 U, whose $M_{rs}(T)/M_s(T)$ vs $M_s(T)$ plot is very noisy, all samples have $m \geq 0.5$. If domain structure were the same at all temperatures, M_{rs}/M_s would be independent of T and m would be zero. The observed non-zero values of m confirm one basic conclusion of paper 1: the number of domains or vortices and/or their structure, for example the positions of domain walls (DWs), must change at elevated temperatures.

Thermally activated remanence unblocking (SD or vortex → SP) accounts for the unusually fast decrease in M_{rs}/M_s with heating in the finest grains; they contain very wide size distributions extending into the SP range. Examples are Wright 4000 (25–65 nm), which gave no meaningful values of n or m because of its broad size spectrum, TK49 and Wright 112 978 (see paper 1, Figs 4 and 5). The other submicron magnetites (5000, 3006, 0.6 U, 1 U) also have quite high m values, from 1.03 to 1.14. Most of these larger grains do not unblock until very close to T_C. Evolving SD and vortex structures must be responsible for the changing M_{rs}/M_s values over the remainder of the temperature range.

The PSD samples of Fig. 2 have the widest range of m values. There is a progression from an MD-like value of 0.5 for 14 U to 0.9 for 3 U (and to 1.0–1.06 for the two 1 μm samples, 1 U and 3006). In Fig. 2(b), data from the one or two highest T steps for four of the samples deviate from the main linear trend, perhaps because of thermal unblocking.

Most samples with $d \geq 20$ μm (04 1183, TK128, 112 982, 110 U) have $m \approx 0.5$–0.7. Of all the size ranges, these MD grains have the least temperature sensitive domain structures. The decrease in M_{rs}/M_s at high T is likely due in part to displacements of existing DWs as a result of decreasing coercivity and wall pinning, rather than to creation of new walls and domains.

Moving to the n values derived from $H_c(T)$ versus $M_s(T)$ plots like those of Fig. 2(a), the expectation that $m = n–1$ (or n—$m = 1$, as tested in Table 2) is met for the 1–14 μm magnetites, with the possible exception of FH3A, and for the MD magnetites, except for 112 982. Thus for the vast majority of MD and PSD size magnetites, $H_c(T)$ and $M_{rs}(T)$ are nearly identical. For the four finest grained samples, however, n—$m > 1$ by 0.4–0.8. Here, the decrease in H_c with increasing T is distinctly more rapid than that of M_{rs}, a hallmark of thermal activation.

5 DEMAGNETIZING FACTOR N FROM H_c AND M_{rs} DATA

MD grains have ramp-like M–H curves with little hysteresis (e.g. TK128: paper 1, Fig. 1d). Their domain walls move readily under the influence of the internal demagnetizing field $\boldsymbol{H}_d = -N\boldsymbol{M}$, where N is the demagnetizing factor, determined mainly by grain shape. N can be estimated from the initial M–H ramp or from ascending and descending branches of the hysteresis loop, which form parallel lines with slopes of $1/N$. For example, between its axis crossing points $M = M_{rs}$, $H = 0$ and $M = 0$, $H = –H_c$, the (linear) descending branch has a slope of $M_{rs}/H_c = 1/N$. Even if the ascending and descending branches are not exactly linear, the ratio M_{rs}/H_c gives an approximate estimate of N.

In two limiting cases, SD grains and MD grains with many domains, demagnetizing factors depend solely on grain shape and the orientation of $\boldsymbol{M}$ relative to the long and short axes. In both these cases, an equidimensional grain has $N = 4\pi/3$ (in cgs emu; 1/3 in SI) and elongated grains have smaller N values (Dunlop & Özdemir 1997, figs 4–5). However, equidimensional grains with only a few domains also have N values $< 4\pi/3$ cgs (Dunlop 1983; Dunlop & Özdemir 1997, figs 5–4, 5–5). 2-domain and 3-domain grains with small wall displacements have $N \approx 2$ (≈ 0.16 in SI), for example. Thus N values $< 4\pi/3$ cgs can indicate either elongated MD (or SD) grains or few-domain structures with broad walls and restricted wall motions.

For large MD grains, N is determined by grain shape alone and should be the same at any temperature. If the linearity of the hysteresis loop between axis crossing points does not change appreciably with T, we should be able to combine $M_{rs}(T)$ and $H_c(T)$ data as in Fig. 3(a) to give straight lines with slopes $1/N$ for the various samples. [Note that $M_s(T_0)$ has been used as a scaling factor so that all samples can be plotted on a single graph.] The data for the MD samples (the third range in Table 2) do indeed define straight lines when M_{rs} and H_c at the same T are plotted against each other in Fig. 3(a). Only at the highest one or two temperatures steps do the data pairs deviate from a straight line.

The N values derived from the slopes in Fig. 3(a) are reasonable. They range from 3 to 4 for the largest grains (Ishpeming and 110 and 135 μm magnetites) to 2.0–2.2 for TK128 and Wright 04 1183 and 112 982 (Table 2). The smaller grains certainly contain fewer domains than the larger grains but greater grain elongation likely causes some of the difference in N values.

Data for PSD-size samples (the second range in Table 2) are plotted in Fig. 3(b). The 20 μm magnetite appears here because its data would fall off scale in Fig. 3(a) but its linearity and N value of 2.8 are like those of the MD samples. The remaining six samples, FH3A and the 3, 6, 9 and 14 μm magnetites, show good data linearity. This is as expected from Figs 2(a) and (b) and Table 2, which demonstrate that these samples have very similar $H_c(T)$ and $M_{rs}(T)$ variations, with $m \approx n$–1. The demagnetizing factors are all close to 2 (Table 1), due to a combination of few domains and moderate elongation (axial ratios of 1.39–1.52, Table 1).

Data for samples from the SD, vortex and lowermost PSD size ranges appear in Fig. 3(c). The plots are at best quasi-linear and those for the two finest-grained samples, Wright 4000 and 112 978, are markedly curved. The line labeled $N = 1.65$ is not intended to define a meaningful demagnetizing factor but to show the curvature of these two plots. Only the two samples with average sizes around 1 μm, Wright 3006 and 1 U, have sufficiently linear plots to yield useful N values: both give $N \approx 2$ (Table 1), like the PSD samples. The non-linearity of most of the plots in Fig. 3(c) comes about because $H_c(T)$ and $M_{rs}(T)$ are not sufficiently alike over most of the T range from 25 to 565 °C, not just near T_C as with the larger magnetites. We anticipated this outcome from the fact that n—m was considerably >1 for the range-1 samples (Table 2). These small grains do not contain well-developed walls which equilibrate in response to the internal demagnetizing field in the way imagined in deriving the relation $M_{rs}/H_c = 1/N$. Their vortex structures have a more SD-like field response, that is rotation of the vortex core moment (Nagy *et al.* 2017). The ascending and descending hysteresis loops are curved between axis crossing points, not linear.

6 GRAIN SIZE DEPENDENCES OF H_c AND M_{rs}/M_s AT CONSTANT T

Figs 4(a) and (b) present H_c and M_{rs}/M_s data in a different way: as a function of grain size d at five temperatures ranging from 25 to 505 °C. The results are from second heating runs when sample magnetic properties had stabilized. The grain size dependences of H_c and M_{rs}/M_s for magnetite are well documented at room temperature (e.g. Dunlop & Özdemir 1997, figs 12.21 and 12.22) and below (Dunlop *et al.* 2019, fig. 8) but Fig. 4 is the first report of variations over a broad size range at high temperature.

The data at all five temperatures define three distinct ranges of grain size. From 0.06 to 0.3 μm, values of H_c and M_{rs}/M_s increase

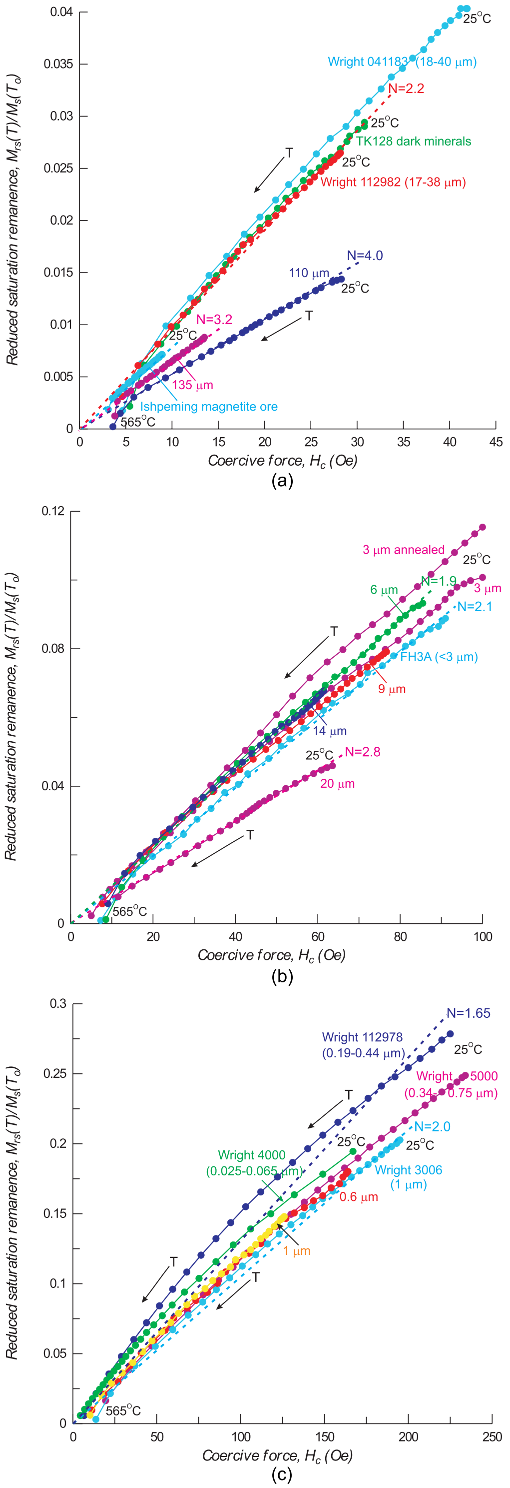

Figure 3. Plots of $M_{rs}(T)$ [normalized by the temperature independent quantity $M_s(T_0)$] versus $H_c(T)$ as a test of eq. (3): $M_{rs}(T) = H_c(T)/N$. (a) MD magnetites obey eq. (3) quite closely, yielding N values of 3–4 cgs for $\geq$ 100 μm grains and 2–3 cgs for 20–40 μm grains (see (b) for the 20 μm data). (b) PSD-size magnetites also display good linearity although they are less obviously described by the self-demagnetization theory on which eq. (3) is based. Their N values of $\approx$2 cgs reflect both elongation (axial ratios of $\approx$1.5) and small numbers of domains. (c) Most magnetites $\leq$1 μm in size are not appropriately described by self-demagnetization theory and accordingly have curved plots from which no meaningful values of N can be deduced. N.B. 1 Oe = 79.6 Am^{-1} (equivalent B: 10^{-4} T).

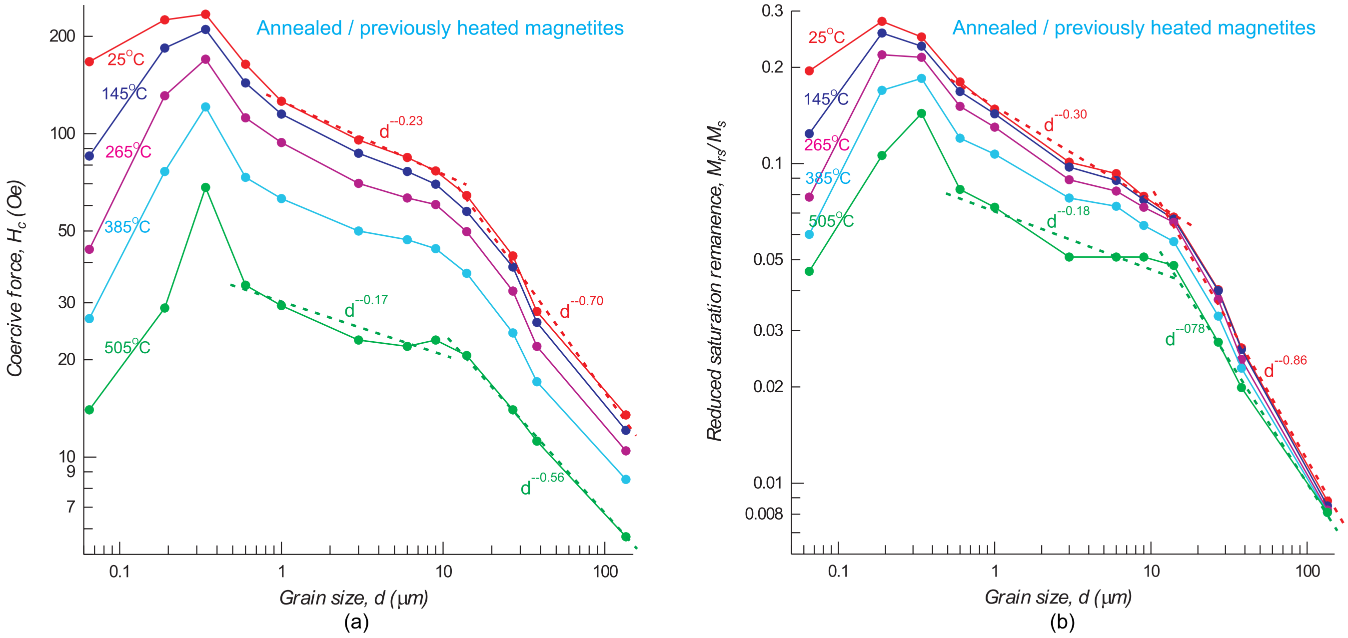

Figure 4. Grain size dependences of (a) H_c and (b) M_{rs}/M_s data measured at selected temperatures between 25 and 505 °C. In the submicron range, values fall with decreasing size d because of broad size distributions in individual samples, which include much SP material with zero coercivity and remanence. In the 0.6–14 μm interval, the data are well described by power laws of $d^{-0.23}$ to $d^{-0.17}$ for H_c and $d^{-0.30}$ to $d^{-0.18}$ for M_{rs}/M_s Above 14 μm, the descents are much steeper, with dependences of $d^{-0.70}$ to $d^{-0.56}$ for H_c and $d^{-0.86}$ to $d^{-0.78}$ for M_{rs}/M_s N.B. 1 Oe = 79.6 Am^{-1} (equivalent B: 10^{-4} T).

with increasing d (Wright samples 4000, 112 978 and 5000), then decrease abruptly between 0.3 and 0.6 μm.

In the second size range, from 0.6 to 14 μm, both H_c and M_{rs}/M_s data decrease steadily with increasing d. The decrease is approximately linear on a log–log plot, giving power-law dependences of $d^{-0.23}$ to $d^{-0.17}$ for H_c and $d^{-0.30}$ to $d^{-0.18}$ for M_{rs}/M_s between 25 and 505 °C. Power-law variations of coercivity and remanence are well documented but those of magnetite are more typically as $d^{-0.4}$ to $d^{-0.5}$ at room temperature (e.g. Parry 1965; Dunlop 1986).

Around 10–15 μm, the data trends change to $d^{-0.70}$ to $d^{-0.56}$ for H_c and $d^{-0.86}$ to $d^{-0.78}$ for M_{rs}/M_s The break is sharp for M_{rs}/M_s, less so for H_c. It may mark the changeover from PSD transitional domain structures—broad walls with limited freedom of motion—to true MD structure, with narrow domain walls whose response to self-demagnetizion is limited only by dislocations and other lattice defects. This third data range extends at least up to 135 μm.

7 DISCUSSION

7.1 Why do M_{rs} and H_c change irreversibly with heating?

There are two main patterns of change in the $H_c(T)$ and $M_{rs}(T)$ curves between heating runs 1 and 2. The first, displayed by FH3A, Ishpeming and Wright 4000 magnetites (Figs 1a, b and e) and also by Wright 112 978 (not illustrated) is an initial rise in both H_c and M_{rs} values to a peak at 105–145 °C in run 1; in run 2, H_c and M_{rs} usually (but not always: e.g. Wright 4000) begin from these peak values; and above 250–300 °C, $H_c(T)$ and $M_{rs}(T)$ from the two runs merge.

Wright 4000 and 112 978 contain submicron size magnetites but have anomalously low $H_c(T_0)$ and $M_{rs}(T_0)$ values (Figs 4a, b), as well as steeply descending $H_c(T)$ and $M_{rs}(T)$ curves that cut across those of other samples (paper 1, figs 4, 5). Because their grain sizes extend into the SP range, a slight increase in size would increase both H_c and M_{rs} substantially, but it is hard to imagine grains sintering at 100–150 °C. On the other hand, van Velzen & Zijderveld (1973) noted that solid-state diffusion of defects would increase by orders of magnitude at 150 °C, accounting for observed changes in coercivity and susceptibility in fine-grained magnetite in marls through removal of oxidized rims on the grains. However, although Wright 4000 and 112 978 have Curie points higher than 580 °C, indicating some surface oxidation, their H_c values increase with heating, while van Velzen & Zijderveld's H_c values decreased.

The second pattern of change in $H_c(T)$ and $M_{rs}(T)$ curves between runs 1 and 2 is displayed by Wright 5000 and 3006 (0.34–1.1 μm), the crushed PQ magnetites (0.6–14 μm), and Wright 04 1183 and 112 982 (20–40 μm). Examples are found in Figs 1(c), (d) and (f) (also in Dunlop 2014, Figs 4a–c). $H_c(T)$ and $M_{rs}(T)$ decrease rapidly in the first heating, then begin to level out between 200 and 300 °C; in run 2, $H_c(T)$ and $M_{rs}(T)$ are well below run 1 values at all T, only merging above 500 °C; run 3, where measured, matches run 2. Except for Wright 5000, $M_s(T)$ and T_C are identical in all runs and match those of pure magnetite.

Kosterov & Prévot (1998) found similar behaviour in some of their basalts, containing ≈1 μm magnetite. H_c decreased in a first heating up to ≈ 200 °C, then recovered, merging with second-heating curves above ≈400 °C. There was no significant chemical change. They attributed the change in coercivity to unspecified changes in domain structure triggered by mild heating.

In the PQ samples a more likely source of coercivity change is annealing out of residual strain produced by crushing the magnetite crystals. Ratios of after-heating to before-heating $H_c(T_0)$ and $M_{rs}(T_0)$ values decrease with decreasing grain size: 84 per cent (14 μm), 78 per cent (9 μm), 72 per cent (6 μm), 63 per cent (3 μm), 60 per cent (1 μm) and 50–55 per cent (0.6 μm). A systematic drop in values is logical as the finer grains were milled for longer times. Dunlop & Özdemir (2018) noted similar reductions in $H_c(T_0)$ and $M_{rs}(T_0)$ after annealing at 700 °C. Heating to only 350 °C seems to be almost as effective in removing obvious anomalies in the heating curves. However, stress/strain reduction must continue well above 350 °C because run-2 H_c and M_{rs} values are reduced relative to run-1 values at temperature steps as high as 545 °C.

Among the Wright magnetites, the ratios are 92 per cent (04 1183, 18–40 μm), 88 per cent (112 982, 17–38 μm), 76 per cent (3006, 1.0–1.1 μm) and 63 per cent (5000, 0.34–0.75 μm). The trend with grain size is like that of the PQ magnetites. 04 1183 and 112 982 are natural magnetites which were probably milled before sizing. 3006 and 5000 are synthetic and may also be strained depending on the method of synthesis.

The practice of pre-annealing samples to stabilize their magnetic properties is not new. It goes back at least as far as the work of Roquet & Thellier (1946). A non-reproducible initial state is surprising in a hydrothermal magnetite like FH3A or bulk magnetite ore like the Ishpeming, however. Every sample studied here changed enough in its first heating to require a second heating run.

7.2 What do numerical relations among $M_{rs}(T)$, $H_c(T)$ and $M_s(T)$ tell us?

Paper 1 reached a number of conclusions about changing domain structures at high T based on a visual comparison of $M_{rs}(T)/M_s(T)$ curves for the entire sample set (paper 1, Fig. 4) and a similar comparison of $H_c(T)$ data (1, fig. 5). A better method is to fit $M_{rs}(T)/M_s(T)$ and $H_c(T)$ data for individual samples to mathematical functions which permit unbiased comparisons among samples. The fitted functions in Figs 2(a) and (b) are power laws of $M_s(T)$, a material property independent of domain structure. The only drawback to this choice is that data measured in the highest temperature steps, where M_s is smallest, have a higher weighting in the line fits because of the logarithmic scales used.

The key questions to be answered are:

(1) How fast and over what range of T does $M_{rs}(T)/M_s(T)$ decrease in various groups of samples?

(2) How fast and over what range of T does $H_c(T)$ decrease in various groups of samples?

(3) How similar to each other are $M_{rs}(T)$ and $H_c(T)$ in individual samples?

(4) What does this tell us about domain/spin structures and coercivity mechanisms at high T?

The answer to question 1 lies in the values of m in the relation $M_{rs}(T)/M_s(T) \sim [M_s(T)]^m$, as calculated from the slopes of data lines in Fig. 2(b) and other similar plots, collected in Table 2. The fits in Fig. 2(b) are convincingly linear up to 505 °C except for FH3A; a single power law describes $M_{rs}(T)/M_s(T)$ at all T and M_{rs}/M_s decreases continuously beginning from 25 °C. The plots for the initially unannealed samples 14 U, 9 U, 6 U and 3 U, plus 1 U and 0.6 U (not shown), form a nested set. However, their m values vary more than a visual inspection of the unfitted $M_{rs}(T)/M_s(T)$ curves had suggested, from ≈ 0.5 for 14 U to 1.06–1.14 for the finest grains (0.6 U and 1 U). In other words, $M_{rs}(T)/M_s(T)$ in the PSD range decreases more rapidly in fine grains and less rapidly in coarser grains. This trend cannot be ascribed to an increased role of thermal activation in finer grains because the line fits utilized data below 505 °C while thermal unblocking in these samples occurs well above 500 °C. The trend suggests two non-thermal mechanisms of changing domain structure at high temperature, their relative importance shifting in finer or coarser grains. DW pinning by different types of lattice defects may play this role, as discussed later in this section.

The trend of less rapidly changing $M_{rs}(T)/M_s(T)$ with increasing grain size is continued into the MD range, where 110 U and 135 U have $m = 0.46$ and 0.24, respectively. The data used for 135 U were from 25 to 365 °C; from 385 to 525 °C, M_{rs}/M_s did not change with heating, that is $m = 0$. Fits for the 20–40 μm samples TK128 and Wright 04 1183 and 1 112 982 also used only part of the data, in this case from 25 to 465 °C. The same is true for the finest grained samples TK49 and Wright 4000, 5000 and 112 978, whose plots were curved (convex down) except below ≈350 °C.

Question 2 is answered by the n values in $H_c(T) \sim [M_s(T)]^n$, determined from the data of Fig. 2(a) and similar plots (Table 2). As with the m values, a single n describes $H_c(T)$ for each of the initially unannealed samples but the n values change from one sample to another. They increase with decreasing grain size from $n = 1.57$ for 14 U to 2.03 for 3 U, and up to 2.54 for 0.6 U. Thus a different mix of coercivity mechanisms must be operative in different sized grains but the mix is the same at all T for each individual sample.

The log H_c versus log M_s plots for the 20–40 μm small MD magnetites are somewhat curved at high T. Line fits over the 25–445 °C interval yield n values of 1.75–1.8, not greatly different from those of the larger PSD magnetites. Plots for 110 U and 135 U are fairly linear up to 505–525 °C and give n values of 1.5 and 1.14, respectively. These large MD grains contain planar domain walls (DWs) whose displacement is the main source of magnetization change. Pinning of DWs by various types and arrays of lattice defects accounts for the coercivity.

Most previous data and modelling have been for 5–15 μm magnetites (Dunlop & Bina 1977; Heider *et al.* 1987; Xu & Merrill 1990; Moskowitz 1993a). Dunlop & Bina (1977) found $n \approx 2$ for their 1–5 μm grains, while Heider *et al.* (1987) reported $n \approx 2.5$ for 12 μm grains. Both are compatible with the n values of 1.8–2.2 for the 0.6–14 μm samples in Table 2. Using the theoretical relation $H_c(T) \sim \lambda_{111}(T)/M_s(T)$ for stress-controlled pinning (Soffel 1970), where λ_{111} is the magnetostriction constant for $\boldsymbol{M_s}$ oriented in the $< 111>$ easy direction of magnetite, with the high-temperature magnetostriction data of Klapel & Shive (1974), Heider *et al.* (1987) found an approximately $M_s{}^2(T)$ dependence for $H_c(T)$, in agreement with their data and most of the PSD results in Table 1. Theories of MD TRM and thermoviscous magnetization have also usually assumed $n = 2$ (Néel 1955; Schmidt 1973; Berndt & Chang 2018).

Xu & Merrill (1992) later showed that DW broadening with rising temperature compromised the effectiveness of wall pinning at high T. Detailed modelling by Moskowitz (1993a, b) for 10 μm magnetite grains yielded a spectrum of possible $H_c(T)$ variations. Only pairs of dislocations interacting with DWs could explain the $n = 2$–2.5 variations measured by Dunlop & Bina (1977) and Heider *et al.* (1987). The same model also accounts for the n values in Table 2 over the PSD range and even beyond, from ≈1.8 for 20–40 μm grains to 2.4–2.5 for 0.3–0.75 and 0.6 μm grains, but not for the n values of the 110 and 135 μm MD magnetites, 1.5 and especially 1.14. Yet these are the grains whose narrow, loosely pinned DWs seem best suited to the modelling.

The close agreement of experimental and theoretical n values over the PSD range implies that even quite small PSD grains behave much like their larger MD counterparts, with DW motion impeded by stresses due to dislocations being the main source of coercivity. If so, is it possible that decreasing $H_c(T)$ drives the observed decreases in M_{rs}/M_s at high temperature? This certainly occurs in large MD grains where the internal demagnetizing field $\boldsymbol{H_d} = —N\boldsymbol{M}$ is able to overcome pinning forces and achieve a re-equilibration of DWs that results in

$$M_{rs}(T) = H_c(T)/N. \tag{3}$$

This equilibrium set of DW positions at any T leads to

$$M_{rs}(T)/M_s(T) = H_c(T)/N M_s(T). \tag{4}$$

Thus decreases in M_{rs}/M_s with rising T would not necessarily imply a change in the number of domains but only a change in their sizes and the positions of their bounding DWs.

This brings us to question 3. If $\boldsymbol{H}_\mathbf{d}$ is able to produce an equilibrium distribution of DW positions in PSD grains, then the ascending and descending hysteresis loop branches between axis crossings should be linear or close to linear, and $M_{rs}(T)$ should mimic $H_c(T)$ as in eq. (3). This is the expectation in relation (1), where the same value n was used *a priori* for both $M_{rs}(T)$ and $H_c(T)$ power laws. It follows from relation (2) that $m = n$–1, that is the expectation value of n—m should be 1, or close to it. All the samples in Table 2 except Wright 112 982 and the <1 μm magnetites indeed have n—$m = 1 \pm 0.16$. This similarity of $M_{rs}(T)$ and $H_c(T)$ data has been observed previously (Levi & Merrill 1978; Dunlop 1987; Heider *et al.* 1987; Yu *et al.* 2004, annealed samples).

The finest magnetites, for which n—$m >> 1$ in Table 2, have tails of ultrafine sizes extending beyond the stable SD range into SP sizes. $H_c(T)$ decreases more rapidly at all T than $M_{rs}(T)$: n ranges from 2.4 to 3.1, whereas $m + 1$ ranges from 2.0 to 2.4. This is a hallmark of thermal activation of SD grains (and possibly of vortices and/or DW moments) below T_{UB}, the thermal unblocking temperature of remanence.

Moving to question 4, what can we deduce about the domain structures responsible for high-temperature changes in H_c and M_{rs}? The broad size distributions of the finest grained samples lead to thermal instability (SD or other state → SP) that effectively masks changes of stable structures, such as SD → vortex. Almost all other samples, spanning the size range 1 μm to 135 μm, seem to contain at least one DW which can move with sufficient freedom in response to self-demagnetization to achieve the equilibrium condition $M_{rs}(T) \approx H_c(T)/N$. Under these circumstances, the decrease in M_{rs}/M_s with rising T, although real, merely mirrors the change in coercivity, that is DW pinning, $H_c(T)$. It is brought about by re-equilibration of sizes of domains through unpinning and repositioning of existing DWs. It does not require a change in numbers of domains, although nucleation of domains could be part and parcel of re-equilibration, as observed by Heider *et al.* (1988) during mild heating.

The smaller PSD grains, in which n and m increase compared to large PSD and MD grains, are fertile ground for multiple mechanisms of coercivity and remanence changes. DWs have permanent moments, which can reverse in SD fashion without affecting the domains they bound (the 'psarks' of Dunlop 1977). If DWs can reverse their moments, so presumably can vortices, albeit with much smaller moments. A single spin vortex occupies much of the volume of the submicron grains investigated by Harrison *et al.* (2002) and Almeida *et al.* (2016). In principle, only the small core region needs to be activated in order to reverse the moment of the grain, although in practice Almeida *et al.* (2016) actually observed reversal of the entire vortex in a 250 nm magnetite grain (from clockwise to counterclockwise) and that occurred only near 600 °C.

Finally, non-equilibrium LEM (local energy minimum) structures, usually with fewer than the equilibrium number of domains, seem to be frequent in small titanomagnetite and pyrrhotite grains (e.g. Halgedahl & Fuller 1983; Boyd *et al.* 1984; Metcalf & Fuller 1987; Halgedahl 1991). Domain nucleation is easy in magnetite, as shown by Heider *et al.* (1988), making metastable LEM states less likely. If they do exist, they likely collapse into the GEM (global energy minimum) state in small reverse fields. In this situation, M_{rs} would be enhanced but H_c would not.

In the larger PSD and MD grains, the n values of 1.5–2, interpreted in the context of DW pinning and unpinning, imply impedance by pairs or arrays of dislocations. Point and planar defects lead to much higher n values (Heider *et al.* 1987; Moskowitz 1993a). The mix of coercivity sources alluded to earlier in this section, which seems to change proportions depending on grain size, is likely between various types and arrangements of dislocations.

7.3 Demagnetizing factors and grain shapes indicated by hysteresis data

The self-demagnetization model used to analyse the temperature variations of H_c and M_{rs}/M_s data from 0.6 to 135 μm magnetites provides an estimate of demagnetizing factor N. Re-equilibration of domain structure by $\boldsymbol{H}_\mathbf{d}$ is embodied in eq. (3), which when rearranged gives

$$N = H_c(T)/M_{rs}(T). \tag{5}$$

Note that the values of N in this paper are in cgs emu; for SI values, divide by 4π.

N depends both on grain elongation ($\boldsymbol{M}_\mathbf{s}$ lying generally along the long axis to minimize $\boldsymbol{H}_\mathbf{d}$) and in few-domain grains, on the number of domains. Two-domain (2D) grains have the smallest value, $N \approx 1.6$, and N increases steadily with increasing domain number to 2 for 3D grains, 2.8 for 4D grains, 3.5 for 8D grains and ultimately 4 to $4\pi/3$ for grains with ≥20 domains (Dunlop & Özdemir 1997, Fig. 5.5). If a sample's average number of domains per grain changes with heating, the resulting change in N will be evident as a change in slope of a plot of $M_{rs}(T)$ versus $H_c(T)$ like Figs 3(a)–(c). Such changes in apparent N have been reported by Dunlop (1987) for 0.076–0.22 μm magnetites and by Argyle & Dunlop (1990) for 0.21–0.54 μm magnetites and interpreted as indicating 2D → 3D and 3D → 4D changes with heating. These changes serve to reduce demagnetizing energy E_d. Although E_d decreases with increasing T as $M_s^2(T)$, the nucleation energy to create a new domain depends on magnetocrystalline anisotropy K, which decreases faster, as a high power of $M_s(T)$ (Dunlop & Özdemir 1997, Chap. 2).

The suite of crushed and centrifuged magnetites (0.6 U through 20 U) have average grain elongations ranging from 1.39 to 1.52 (Table 1), corresponding to $N = 2.83$–3.14 for large MD grains (Dunlop & Özdemir 1997, Fig. 4.5). The N values calculated from H_c/M_{rs} data for 1 U through 14 U vary from 1.8 to 2.1 with no particular pattern with respect to grain size (Table 2). These are lower than large MD values because these grains contain many fewer than 20 domains. On the other hand, 20 U has a calculated N of 2.8 which matches the limiting MD value $N = 2.83$ for its axial ratio of 1.52. 110 U and 135 U, which contain equant grains, have inferred N values of 4.0 and 3.2, respectively, fairly close to the expected 4 to $4\pi/3$ for large MD grains.

There is no pattern of gradually changing N (i.e. H_c/M_{rs}) with rising T like that reported by Dunlop (1987) and Argyle & Dunlop (1990) for 0.08–0.54 μm magnetites. This would be manifest as a steady increase or decrease in slope of $M_{rs}(T)$ versus $H_c(T)$ plots with increasing T. In fact most MD and PSD samples plot very close to straight lines through the origin in Figs 3(a) and (b), apart from some deviations above 500 °C caused by the H_c residuals noted in Section 3.

7.4 What do grain size dependences of H_c and M_{rs}/M_s tell us?

Having deduced in Section 7.2 that changes in H_c may be driving changes in M_{rs}/M_s, it is logical to examine how H_c varies with d and then see to what extent the size variation of M_{rs}/M_s mimics $H_c(d)$. Most theories and previous data concern $H_c(d)$ at room temperature (Stacey 1963; Parry 1965; Stacey & Wise 1967; Soffel 1970; Rahman *et al.* 1973; Hartstra 1982; Xu & Merrill 1990). H_c values for a specific grain size of magnetite are an order of magnitude higher for crushed/stressed grains (van Oosterhout & Klomp 1962; Day *et al.* 1977; Worm & Markert 1987), even annealed (Parry 1965; Dankers & Sugiura 1981; Dunlop *et al.* 2019), than for hydrothermally grown low-stress crystals (Dunlop 1986; Heider *et al.* 1987; Argyle & Dunlop 1990; Muxworthy 2002).

The room-temperature H_c and M_{rs}/M_s data of the crushed magnetites in this study, even after a first heating to 585 °C, fall closer to the established data trends for stressed material than to the hydrothermal/low-stress data (Dunlop *et al.* 2019, Fig. 4; Dunlop & Özdemir 2015, Fig. 19). The hydrothermal H_c data fall along a single line of slope ≈ –0.6 on a bilogarithmic plot of H_c versus d from SD sizes (0.04 µm) to 1000 µm (Heider *et al.* 1987). The sets of stressed and partially annealed magnetites have bilogarithmic plots that change slope (e.g. Dunlop 1986) at grain sizes that have been interpreted as marking a transition from PSD to true MD behaviour (e.g. Stacey 1962, 1963).

Above room temperature, the present crushed magnetite H_c and M_{rs}/M_s data also define lines on bilogarithmic grain size plots (Figs 4a and b). At 25 °C, over the range 0.6 µm $\leq d \leq$ 14 µm, $H_c(d)$ varies as $d^{-0.23}$ while $M_{rs}/M_s \sim d^{-0.30}$. As T increases the line slopes decrease, reaching $H_c \sim d^{-0.17}$ and $M_{rs}/M_s \sim d^{-0.18}$ at 505 °C. The similarity of $H_c(d)$ and $M_{rs}(d)$ size dependences at a variety of temperatures favours control of M_{rs} by H_c through self-demagnetization, in the manner of eqs (3) and (4). H_c leads and M_{rs}/M_s follows.

It may seem surprising that a self-demagnetization model invoking the re-equilibration of DWs works so well in small PSD grains, where there can only be room for a few DWs and the walls fill a significant fraction of the grain volume. Self-demagnetization does not require DW displacements, only a change of total net moment. Rotation of domain magnetizations serves the purpose, although the perpendicular susceptibility due to rotation is lower than the susceptibility due to fields parallel to the domain magnetizations (Stacey 1963; Stacey & Banerjee 1974). In addition, magnetic vortices in >1 µm magnetite grains may possibly respond to $\boldsymbol{H}_{\mathbf{d}}$ in such a way as to generate relations like (3) and (4) between M_{rs} and H_c, although a mechanism remains to be demonstrated.

Grains smaller than 0.6 µm do not continue the same size dependences in Figs 4(a) and (b). Instead H_c and M_{rs}/M_s rise sharply to peaks as d decreases, then decline with further decreases in d. The peak values of M_{rs}/M_s in Fig. 4(b) are 0.2–0.3, compared to $M_{rs}/M_s = 0.5$ for SD grains with shape anisotropy. Rather than a peak around 0.3 µm, further increases might have been expected as d decreases towards the SD threshold $d_0 \sim$ 0.06–0.08 µm (Dunlop & Özdemir 1997, Table 5–1).

Vortices cannot be responsible for the remanence peak because they have only small net moments due to a central core region. Nor can they explain the coercivity peak. To reverse the core magnetization by coherent rotation would require SD-like coercivities but grains this large likely have lower-coercivity incoherent reversal modes, for example curling. PSD grains likewise cannot explain the peak in H_c. Bloch walls do not begin to develop until sizes larger than 0.3 µm (Nagy *et al.* 2019. Moreover, although they have SD-like moments of $(2/\pi)VM_s$, where V is DW volume, they too can reverse incoherently, by low-H_c Bloch-line propagation (Dunlop 1977).

The peaks actually result from anomalously low H_c and M_{rs}/M_s values of the two samples with mean sizes < 0.3 µm (4000 and 112 978), whose broad size distributions extend below the SP threshold of 0.025–0.03 µm (Dunlop & Özdemir 1997, table 5-1). Maher (1988), in room-temperature measurements, found similar peaks below 1 µm due to ultrafine SP magnetite. At 265, 385 and 505 °C, the H_c and M_{rs}/M_s peaks in Figs 4(a) and (b) become more accentuated. With rising T, as more grains are thermally activated and become SP, the H_c and M_{rs}/M_s values of 112 978 and especially 4000 plummet, enhancing the 0.3 µm peak.

The interaction of DWs with dislocations and other lattice defects leads naturally to a d^{-p} dependence for H_c with a wide range of possible p values depending on the details of the interaction (Stacey 1963; Stacey & Wise 1967). Measured dislocation densities in some of Heider *et al.*'s (1987) magnetite crystals when used in Stacey & Wise's (1967) and Soffel's (1970) models gave H_c values in good agreement with those observed. Room-temperature experimental values for p are ≈ 0.6 for hydrothermal magnetites (Heider *et al.* 1987) and 0.4–0.5 for magnetites with more internal strain (Parry 1965; Dunlop 1986). The p values for 0.6–14 µm magnetites in Fig. 4(a) are much lower: 0.23 at 25 °C, dropping to 0.17 at 505 °C. Higher values, 0.70 at 25 °C to 0.56 at 505 °C, are found for the 14–135 µm size range.

8 CONCLUSIONS

The principal conclusions of this study are the following:

(1) M_{rs}/M_s decreases at high T in magnetites of all grain sizes. There are three possible causes:

(i) thermal activation/unblocking;
(ii) changing domain structure: nucleation/denucleation, SD ↔ vortex ↔ DW
(iii) re-equilibration, for example repositioning of DWs

(2) H_c also decreases at high T. For PSD (1–15 µm) and MD (15–135 µm) magnetites, H_c and M_{rs} have similar experimental temperature dependences: $M_{rs}(T) \sim H_c(T)$. This observation favours re-equilibration of domains at high T, with or without nucleation of new domains.

(3) For <1 µm magnetites, with predominantly SD and vortex structures, $H_c(T)$ decreases more rapidly than $M_{rs}(T)$, as expected for thermal activation below the remanence T_{UB}. SD ↔ vortex ↔ DW transitions are neither strongly supported nor ruled out by the data.

(4) These conclusions, based on visual comparisons in an earlier paper (Dunlop 2021), have been made quantitative by mathematical fitting: $H_c(T), \sim [M_s(T)]^n$, $M_{rs}(T)/M_s(T) \sim [M_s(T)]^m$.

(5) Grain size dependences $M_{rs}(d)$ and $H_c(d)$ have been measured for the first time at elevated temperatures, from T_0 to near T_C, over the broad range 0.025–135 µm.

(6) $M_{rs}(d)$ and $H_c(d)$ show clear divisions into SD/vortex (<0.6 µm), PSD (0.6–15 µm) and MD (>15 µm) regions. The boundaries do not shift notably between 25 and 505 °C, implying no gross changes in domain structure ranges up to 505 °C.

(7) $M_{rs}(d)$ and $H_c(d)$ have similar power-law variations at each T: $M_{rs}(d) \sim H_c(d)$. This is further support for re-equilibration driven

by self-demagnetization. Different power laws hold in the PSD and MD regions.

(8) Self-demagnetization leads to a simple formula for demagnetizing factor N:

$$N = H_c(T)/M_{rs}(T).$$

Calculated N values for PSD and MD samples are reasonably T independent. N values (cgs) for 1–14 μm magnetites are 1.8–2.1 (Table 2), lower than theoretical MD values N = 2.83–3.14 for their axial ratios (1.4–1.5) because of their small number of domains. Larger grains (20, 110 and 135 μm) with more domains have N = 2.8, 4.0 and 3.2, respectively, compared to theoretical values of 2.83–$4\pi/3$ (axial ratios: 1 to 1.5).

(9) True $M_{rs}(T)$ and $H_c(T)$ variations are only seen in a second heating. A 15–50 per cent reduction of M_{rs} and H_c at all T occurs in crushed natural crystals. The largest changes are in the finest grains. Magnetites from low-stress environments (hydrothermal, massive ores) can also show significant changes in their first heating.

ACKNOWLEDGEMENTS

Measurements were made at the Institute of Rock Magnetism, which operates with support from the National Science Foundation, Earth Sciences Division and the University of Minnesota. Subir Banerjee and Bruce Moskowitz hosted the visits and Mike Jackson, Jim Marvin and Peat Sølheid gave help with instruments and programs. Franz Heider, Joseph Hodych and Özden Özdemir helped obtain samples. Song Xu separated the crushed magnetites and measured their size spectra. Thanks to Mark Dekkers and editor Eduard Petrovsky for valuable suggestions. Data in this paper are available from the author on request. Research supported by the Natural Sciences and Engineering Research Council of Canada.

REFERENCES

Almeida, T.P. *et al.*, 2016. Direct observation of the thermal demagnetization of magnetic vortex structures in nonideal magnetite recorders, *Geophys. Res. Lett.,* **43,** 8426–8434.

Ambatiello, A., Fabian, K. & Hoffmann, V., 1999. Magnetic domain structure of multidomain magnetite as a function of temperature: observations by Kerr microscopy, *Phys. Earth planet. Inter.,* **112,** 55–80.

Argyle, K. & Dunlop, D.J., 1990. Low-temperature and high-temperature hysteresis of small multidomain magnetites (215-540 nm), *J. geophys. Res.,* **95,** 7083–7096.

Berndt, T.A. & Chang, L., 2018. Theory of stable multi-domain thermoviscous remanence based on repeated domain-wall jumps, *J. geophys. Res.,* **123,** doi: 10.1029/2018JB016816.

Boyd, J.R., Fuller, M. & Halgedahl, S.L., 1984. Domain wall nucleation as a controlling factor in the behavior of fine magnetic particles in rocks, *Geophys. Res. Lett.,* **11,** 193–196.

Carter-Stiglitz, B., Moskowitz, B., Solheid, P., Berquó, T.S., Jackson, M. & Kosterov, A., 2006. Low-temperature magnetic behavior of multidomain titanomagnetites: TM0, TM16, and TM35, *J. geophys. Res.,* **111,** B12S05, doi:10.1029/2006JB004561.

Dankers, P. & Sugiura, N., 1981. The effects of annealing and concentration on the hysteresis properties of magnetite around the PSD-MD transition, *Earth planet. Sci. Lett.,* **56,** 422–428.

Day, R., Fuller, M. & Schmidt, V.A., 1977. Hysteresis properties of titanomagnetites: grain size and compositional dependence, *Phys. Earth planet. Inter.,* **13,** 260–267.

Dunlop, D.J., 1977. The hunting of the ‘psark’, *J. Geomagn. Geoelectr.,* **29,** 293–318.

Dunlop, D.J., 1983. On the demagnetizing energy and demagnetizing factor of a multidomain ferromagnetic cube, *Geophys. Res. Lett.,* **10,** 79–82.

Dunlop, D.J., 1986. Hysteresis properties of magnetite and their dependence on particle size: a test of pseudo-single-domain remanence models, *J. geophys. Res.,* **91,** 9569–9584.

Dunlop, D.J., 1987. Temperature dependence of hysteresis in 0.04-0.22 μm magnetites and implications for domain structure, *Phys. Earth planet. Inter.,* **46,** 100–119.

Dunlop, D.J., 2014. High-temperature susceptibility of magnetite: a new pseudo-single-domain effect, *Geophys. J. Int.,* **199,** 707–716.

Dunlop, D.J., 2021. Magnetic hysteresis of magnetite, pyrrhotite and hematite at high temperature, *Geophys. J. Int.,* **225,** 1–14, fast link https://academic.oup.com/gji/advance-article/doi/10.1093/gji/ggaa569/6032169?guestAccessKey=61e8fb2d-63fe-4011-a9b2-bfaf9259c329.

Dunlop, D.J. & Bina, M-M., 1977. The coercive force spectrum of magnetite at high temperatures: evidence for thermal activation below the blocking temperature, *Geophys. J. R. astr. Soc.,* **51,** 121–147.

Dunlop, D.J. & Özdemir, Ö., 1997. *Rock Magnetism: Fundamentals and Frontiers: Cambridge Studies in Magnetism,* Vol., **3,** 573pp., Cambridge Univ. Press.

Dunlop, D.J. & Özdemir, Ö., 2015. Magnetizations in rocks and minerals, Chap. 5.08in *Treatise on Geophysics, Vol. 5 – Geomagnetism,* 2nd edn, pp. 255–308, ed. Schubert, G., Elsevier.

Dunlop, D.J. & Özdemir, Ö., 2018. Remanence cycling of 0.6-135 μm magnetites across the Verwey transition, *Earth Planets Space,* **70,** 164–177, fast link https://rdcu.be/8AAg.

Dunlop, D.J., Özdemir, Ö. & Xu, S., 2019. Magnetic hysteresis of 0.6–110 μm magnetites across the Verwey transition, *Can. J. Earth Sci.,* **56,** 958–972.

Dunlop, D.J., Zhang, B. & Özdemir, Ö., 2005. Linear and non-linear Thellier paleointensity behavior of natural minerals, *J. geophys. Res.,* **110,** B01103, doi:10.1029/JB2004003095.

Everitt, C.W.F., 1962. Thermoremanent magnetization III. Theory of multidomain grains, *Phil. Mag.,* **7,** 599–616.

Geiss, C.E., Heider, F. & Soffel, H.C., 1996. Magnetic domain observations on magnetite and titanomaghemite grains (0.5–10 μm), *Geophys. J. Int.,* **124,** 75–88.

Halgedahl, S.L., 1991. Magnetic domain patterns observed on synthetic Ti-rich titanomagnetite as a function of temperature and in states of thermoremanent magnetization, *J. geophys. Res.,* **96,** 3943–3972.

Halgedahl, S.L. & Fuller, M., 1983. The dependence of magnetic domain structure upon magnetization state with emphasis on nucleation as a mechanism for pseudo-single-domain behavior, *J. geophys. Res.,* **88,** 6505–6522.

Harrison, R.J., Dunin-Borkowski, R.E. & Putnis, A., 2002. Direct imaging of nanoscale magnetic interactions in minerals, *Proc. Natl. Acad. Sci. U.S.A.,* **99,** 16556–16561.

Hartstra, R.L., 1982. Grain size dependence of initial susceptibility and saturation magnetization related parameters of four natural magnetites in the PSD-MD range, *Geophys. J. R. astr. Soc.,* **71,** 477–495.

Heider, F., Dunlop, D.J. & Sugiura, N., 1987. Magnetic properties of hydrothermally recrystallized magnetite crystals. *Science,* **236,** 1287–1290.

Heider, F., Halgedahl, S.L. & Dunlop, D.J., 1988. Temperature dependence of magnetic domains in magnetite crystals, *Geophys. Res. Lett.,* **15,** 499–502.

Jackson, M., Worm, H-U. & Banerjee, S.K., 1990. Fourier analysis of digital hysteresis data: rock magnetic applications, *Phys. Earth planet. Inter.,* **65,** 78–87.

Klapel, G.D. & Shive, P.N., 1974. High-temperature magnetostriction of magnetite, *J. geophys. Res.,* **79,** 2629–2633.

Kosterov, A.A. & Prévot, M., 1998. Possible mechanisms causing failure of Thellier palaeointensity experiments in some basalts, *Geophys. J. Int.,* **134,** 554–572.

Levi, S. & Merrill, R.T., 1978. Properties of single-domain, pseudo-single-domain and multidomain magnetite, *J. geophys. Res.,* **83,** 309–323.

Maher, B.A., 1988. Magnetic properties of some synthetic submicron magnetites, *Geophys. J.,* **94,** 83–96.

Metcalf, M. & Fuller, M., 1987. Domain observations of titanomagnetites during hysteresis at elevated temperatures and thermal cycling, *Phys. Earth planet. Inter.,* **46,** 120–126.

Moskowitz, B.M., 1993a. Micromagnetic study of the influence of crystal defects on coercivity in magnetite, *J. geophys. Res.,* **98,** 18011–18026.

Moskowitz, B.M., 1993b. High-temperature magnetostriction of magnetite and titanomagnetites, *J. geophys. Res.,* **98,** 359–371.

Muxworthy, A.R., 2002. Magnetic hysteresis and rotational hysteresis of properties of hydrothermally grown multidomain magnetite, *Geophys. J. Int.,* **149,** 101–114.

Nagy, L., Williams, W., Muxworthy, A.R., Fabian, K., Almeida, T.P., Conbhuiu, P. & Shcherbakov, V.P., 2017. Stability of equidimensional pseudo-single-domain magnetite over billion year timescales, *Proc. nat. Acad. Sci. U.S.A.,* **114,** 10356–10360.

Nagy, L., Williams, W., Tauxe, L. & Muxworthy, A.R., 2019. From nano to micro: evolution of magnetic domain structures in multidomain magnetite, *Geochem. Geophys. Geosyst.,* **20,** 2907–2918.

Néel, L., 1955. Some theoretical aspects of rock magnetism, *Adv. Phys.,* **4,** 191–243.

Özdemir, Ö. & Dunlop, D.J., 2006. Magnetic domain observations on magnetite crystals in biotite and hornblende grains, *J. geophys. Res.,* **111,** B06103, doi:10.1029/2005JB004090.

Pan, Q., Pokhil, T.G. & Moskowitz, B.M., 2002. Domain structures in epitaxial Fe_3O_4 particles studied by magnetic force microscopy, *J. appl. Phys.,* **91,** 5945–5950.

Parry, L.G., 1965. Magnetic properties of dispersed magnetite powders, *Phil. Mag.,* **11,** 303–312.

Rahman, A.A., Duncan, A.D. & Parry, L.G., 1973. Magnetization of multidomain magnetite particles, *Riv. Ital. Geofis.,* **22,** 139–146.

Roberts, A.P. *et al.*, 2017. Resolving the origin of pseudo-single-domain behavior, *J. geophys. Res.,* **122,** 9534–9558.

Roquet, J. & Thellier, E., 1946. Sur les lois numériques simples, relatives à l'aimantation thermorémanente du sesquioxyde de fer rhomboédrique, *C. R. Acad. Sci. Paris,* **222,** 1288–1290.

Schmidt, V.A., 1973. A multidomain model of thermoremanence, *Earth planet. Sci. Lett.,* **20,** 440–446.

Soffel, H.C., 1970. The influence of dislocation density and inclusions on the coercive force of multidomain titanomagnetites of the composition $0.65Fe_2TiO_4$ –$0.35Fe_3O_4$ in basalts as deduced from domain structure observations, *Z. Geophys.,* **36,** 113–124.

Stacey, F.D., 1962. A generalized theory of thermoremanence, covering the transition from single domain to multi-domain magnetic grains, *Phil. Mag.,* **7,** 1887–1900.

Stacey, F.D., 1963. The physical theory of rock magnetism, *Adv. Phys.,* **12,** 45–133.

Stacey, F.D. & Banerjee, S.K., 1974. *The Physical Principles of Rock Magnetism,* 195pp., Elsevier.

Stacey, F.D. & Wise, K.N., 1967. Crystal dislocations and coercivity in fine grained magnetite, *Aust. J. Phys.,* **20,** 507–513.

van Velzen, A.J. & Zijderveld, J.D.A., 1973. Effects of weathering on single-domain magnetite in Early Pliocene marine marls, *Geophys. J. Int.,* **121,** 267–278.

van Oosterhout, G.W. & Klomp, C.J., 1962. The effect of grinding on the coercive force of magnetite, *Appl. Sci. Res.,* **9,** 288–290.

Worm, H-U. & Markert, H, 1987. Magnetic hysteresis properties of fine particle titano-magnetites precipitated in a silicate matrix, *Phys. Earth planet. Inter.,* **46,** 84–92.

Xu, S. & Merrill, R.T., 1990. Microcoercivity, bulk coercivity and saturation remanence in multidomain materials, *J. geophys. Res.,* **95,** 7083–7090.

Xu, S. & Merrill, R.T., 1992. Stress, grain size and magnetic stability of magnetite, *J. geophys. Res.,* **97,** 4321–4329.

Yu, Y., Dunlop, D.J. & Özdemir, Ö., 2002. Partial anhysteretic remanent magnetization in magnetite, 1. Additivity, *J. geophys. Res.,* **107**(B10), 2244, doi:10.1029/2001JB001249.

Yu, Y., Tauxe, L. & Moskowitz, B.M., 2004. Temperature dependence of magnetic hysteresis, *Geochem. Geophys. Geosyst.,* **5**(6), Q06H11, doi:10.1029/2003GC000685.

Key words

Authors are requested to choose key words from the list below to describe their work. The key words will be printed underneath the summary and are useful for readers and researchers. Key words should be separated by a semi-colon and listed in the order that they appear in this list. An article should contain no more than six key words.

COMPOSITION and PHYSICAL PROPERTIES

Composition and structure of the continental crust
Composition and structure of the core
Composition and structure of the mantle
Composition and structure of the oceanic crust
Composition of the planets
Creep and deformation
Defects
Elasticity and anelasticity
Electrical properties
Equations of state
Fault zone rheology
Fracture and flow
Friction
High-pressure behaviour
Magnetic properties
Microstructure
Permeability and porosity
Phase transitions
Plasticity, diffusion, and creep

GENERAL SUBJECTS

Core
Gas and hydrate systems
Geomechanics
Geomorphology
Glaciology
Heat flow
Hydrogeophysics
Hydrology
Hydrothermal systems
Infrasound
Instrumental noise
Ionosphere/atmosphere interactions
Ionosphere/magnetosphere interactions
Mantle processes
Ocean drilling
Structure of the Earth
Thermochronology
Tsunamis
Ultra-high pressure metamorphism
Ultra-high temperature metamorphism

GEODESY and GRAVITY

Acoustic-gravity waves
Earth rotation variations
Geodetic instrumentation
Geopotential theory
Global change from geodesy
Gravity anomalies and Earth structure
Loading of the Earth
Lunar and planetary geodesy and gravity
Plate motions
Radar interferometry
Reference systems
Satellite geodesy
Satellite gravity
Sea level change
Seismic cycle
Space geodetic surveys
Tides and planetary waves
Time variable gravity
Transient deformation

GEOGRAPHIC LOCATION

Africa
Antarctica
Arctic region
Asia
Atlantic Ocean
Australia
Europe
Indian Ocean
Japan
New Zealand
North America
Pacific Ocean
South America

GEOMAGNETISM and ELECTROMAGNETISM

Archaeomagnetism
Biogenic magnetic minerals
Controlled source electromagnetics (CSEM)
Dynamo: theories and simulations
Electrical anisotropy
Electrical resistivity tomography (ERT)
Electromagnetic theory
Environmental magnetism
Geomagnetic excursions
Geomagnetic induction
Ground penetrating radar
Magnetic anomalies: modelling and interpretation
Magnetic fabrics and anisotropy
Magnetic field variations through time
Magnetic mineralogy and petrology
Magnetostratigraphy
Magnetotellurics
Marine electromagnetics
Marine magnetics and palaeomagnetics
Non-linear electromagnetics
Palaeointensity
Palaeomagnetic secular variation
Palaeomagnetism
Rapid time variations
Remagnetization
Reversals: process, time scale, magnetostratigraphy
Rock and mineral magnetism
Satellite magnetics

GEOPHYSICAL METHODS

Downhole methods
Fourier analysis
Fractals and multifractals
Image processing
Instability analysis
Interferometry
Inverse theory
Joint inversion
Neural networks, fuzzy logic
Non-linear differential equations
Numerical approximations and analysis
Numerical modelling
Numerical solutions
Persistence, memory, correlations, clustering
Probabilistic forecasting
Probability distributions
Self-organization
Spatial analysis
Statistical methods
Thermobarometry
Time-series analysis
Tomography
Waveform inversion
Wavelet transform

PLANETS

Planetary interiors
Planetary volcanism

SEISMOLOGY

Acoustic properties
Body waves
Coda waves
Computational seismology
Controlled source seismology
Crustal imaging
Earthquake dynamics
Earthquake early warning
Earthquake ground motions
Earthquake hazards
Earthquake interaction, forecasting, and prediction
Earthquake monitoring and test-ban treaty verification
Earthquake source observations
Guided waves
Induced seismicity
Interface waves
Palaeoseismology
Rheology and friction of fault zones
Rotational seismology
Seismic anisotropy
Seismic attenuation
Seismic instruments
Seismic interferometry
Seismicity and tectonics
Seismic noise
Seismic tomography
Site effects
Statistical seismology
Surface waves and free oscillations
Theoretical seismology

Tsunami warning
Volcano seismology
Wave propagation
Wave scattering and diffraction

TECTONOPHYSICS

Backarc basin processes
Continental margins: convergent
Continental margins: divergent
Continental margins: transform
Continental neotectonics
Continental tectonics: compressional
Continental tectonics: extensional
Continental tectonics: strike-slip and transform
Cratons
Crustal structure
Diapirism
Dynamics: convection currents, and mantle plumes
Dynamics: gravity and tectonics
Dynamics: seismotectonics
Dynamics and mechanics of faulting
Dynamics of lithosphere and mantle
Folds and folding
Fractures, faults, and high strain deformation zones
Heat generation and transport
Hotspots
Impact phenomena
Intra-plate processes
Kinematics of crustal and mantle deformation
Large igneous provinces
Lithospheric flexure
Mechanics, theory, and modelling
Microstructures
Mid-ocean ridge processes
Neotectonics
Obduction tectonics
Oceanic hotspots and intraplate volcanism
Oceanic plateaus and microcontinents
Oceanic transform and fracture zone processes
Paleoseismology
Planetary tectonics
Rheology: crust and lithosphere
Rheology: mantle
Rheology and friction of fault zones
Sedimentary basin processes
Subduction zone processes
Submarine landslides
Submarine tectonics and volcanism
Tectonics and climatic interactions
Tectonics and landscape evolution
Transform faults
Volcanic arc processes

VOLCANOLOGY

Atmospheric effects (volcano)
Calderas
Effusive volcanism
Eruption mechanisms and flow emplacement
Experimental volcanism
Explosive volcanism
Lava rheology and morphology
Magma chamber processes
Magma genesis and partial melting
Magma migration and fragmentation
Mud volcanism
Physics and chemistry of magma bodies
Physics of magma and magma bodies
Planetary volcanism
Pluton emplacement
Remote sensing of volcanoes
Subaqueous volcanism
Tephrochronology
Volcanic gases
Volcanic hazards and risks
Volcaniclastic deposits
Volcano/climate interactions
Volcano monitoring
Volcano seismology

© 2017 RAS, *GJI*